Constraints on the magnitude and patterns of ocean cooling at the Last Glacial Maximum

C. Waelbroeck, A. Paul, Michal Kucera, Antoni Rosell-Melé, Mara Weinelt, Ralph Schneider, Alan C. Mix, Andrea Abelmann, Leanne Armand, Edouard Bard, et al.

nature geoscience

LETTERS

PUBLISHED ONLINE: 18 JANUARY 2009 | DOI: 10.1038/NGEO411

Constraints on the magnitude and patterns of ocean cooling at the Last Glacial Maximum

MARGO Project Members*

Observation-based reconstructions of sea surface temperature from relatively stable periods in the past, such as the Last Glacial Maximum, represent an important means of constraining climate sensitivity and evaluating model simulations[1]. The first quantitative global reconstruction of sea surface temperatures during the Last Glacial Maximum was developed by the Climate Long-Range Investigation, Mapping and Prediction (CLIMAP) project in the 1970s and 1980s (refs 2,3). Since that time, several shortcomings of that earlier effort have become apparent[4]. Here we present an updated synthesis of sea surface temperatures during the Last Glacial Maximum, rigorously defined as the period between 23 and 19 thousand years before present, from the Multiproxy Approach for the Reconstruction of the Glacial Ocean Surface (MARGO) project[5]. We integrate microfossil and geochemical reconstructions of surface temperatures and include assessments of the reliability of individual records. Our reconstruction reveals the presence of large longitudinal gradients in sea surface temperature in all of the ocean basins, in contrast to the simulations of the Last Glacial Maximum climate available at present[6,7].

Studies following the Climate Long-Range Investigation, Mapping and Prediction (CLIMAP) project mainly reanalysed old primary data, applied single new proxies or concentrated on specific ocean basins[8–11]. The Multiproxy Approach for the Reconstruction of the Glacial Ocean Surface (MARGO) project's objective has been to compile and analyse available estimates of Last Glacial Maximum (LGM) sea surface temperatures (SSTs) based on all prevalent microfossil-based (transfer functions based on planktonic foraminifera, diatom, dinoflagellate cyst and radiolarian abundances) and geochemical (alkenones and planktonic foraminifera Mg/Ca) palaeothermometers. The MARGO project approach is to argue that no current proxy method is objectively better than another to provide an accurate picture of past SST, and that consequently the multiproxy approach yields the least biased representation of past reality. By using a rigorous definition of the LGM time interval (19–23 cal kyr BP; ref. 4), many records used previously had to be discarded. Other key features are the use of a common data set of ambient temperatures for the calibration of all proxies and the assessment of the reliability of individual SST estimates[5].

The MARGO compilation combines 696 individual SST reconstructions (Fig. 1). The coverage is especially dense in the North Atlantic, the Southern Ocean and the tropics. Several oceanic regions remain undersampled, such as the subtropical gyres, especially in the Pacific Ocean. Individual proxies have different spatial coverage and analyses of multiple palaeothermometers on the same material remain rare. To address this spatial bias, we have projected the entire SST data set onto a regular grid of $5° \times 5°$ resolution (Figs 1 and 2). Each grid cell has been assigned an SST estimate by averaging individual proxy reconstructions that fall into the same cell, weighted by their mean reliability index (see the Methods section and Supplementary Information). The uncertainty associated with the resulting multiproxy SST reconstruction has been computed considering the differences between the single proxy reconstructions in each grid cell (see the Methods section). The choice of the grid size is a compromise enabling us to assess the divergence of multiple SST estimates within each grid cell, as well as to resolve spatial SST gradients in different ocean basins.

The resulting SST anomalies (LGM–World Ocean Atlas (WOA) SST; ref. 12) exhibit an array of robust spatial and seasonal features (Figs 2–4). There is an overall agreement in the magnitude of the latitudinal anomalies between geochemical and microfossil proxies (Fig. 3g,h). As originally suggested by CLIMAP, the strongest annual mean cooling (up to $-10\,°C$) occurred in the mid-latitude North Atlantic and extended into the western Mediterranean ($-6\,°C$, Fig. 2). However, in contrast to CLIMAP, MARGO data indicate that the cooling was more pronounced in the eastern than in the western basin. The magnitude and position of a steep temperature gradient between 45 and 60° N are supported by four different proxies, confirming the robustness of previous single proxy reconstructions in this region[3,10,11] (Fig. 3a,b). Existing coupled atmosphere–ocean general circulation model (AO-GCM) simulations for the LGM show significant disagreement with respect to the location and magnitude of the North Atlantic cold anomaly[6] while exhibiting stronger glacial cooling in the western than in the eastern Atlantic (http://pmip2.lsce.ipsl.fr/) (ref. 7). This demonstrates that the robust MARGO North Atlantic east–west SST anomaly gradient is a good target with which the skill of models can be evaluated.

In contrast with the CLIMAP reconstruction, all proxies also agree on ice-free conditions in the Nordic seas during glacial summer[13]. However, large discrepancies with respect to glacial temperatures recorded by different microfossil proxies remain (Fig. 3a). Positive anomalies derived from dinocyst transfer functions have been interpreted as representing a 'no-analogue' situation under partial sea ice coverage and glacial wind fields[13]. In contrast, foraminifera-based estimates seem to be consistent with glacial oxygen isotope patterns[14]. However, there is at present no objective way to reconcile the divergent proxy results and thus, paradoxically, the glacial conditions in the most densely sampled Nordic seas remain associated with large uncertainties. In contrast to the North Atlantic, some areas of the glacial Northwest Pacific seem to have been slightly warmer at the LGM than at present. These results are based mainly on alkenone unsaturation ratios ($U^{K'}_{37}$) and, rather than a warm anomaly in the annual mean SST values, they

*A full list of authors and their affiliations appears at the end of the paper.

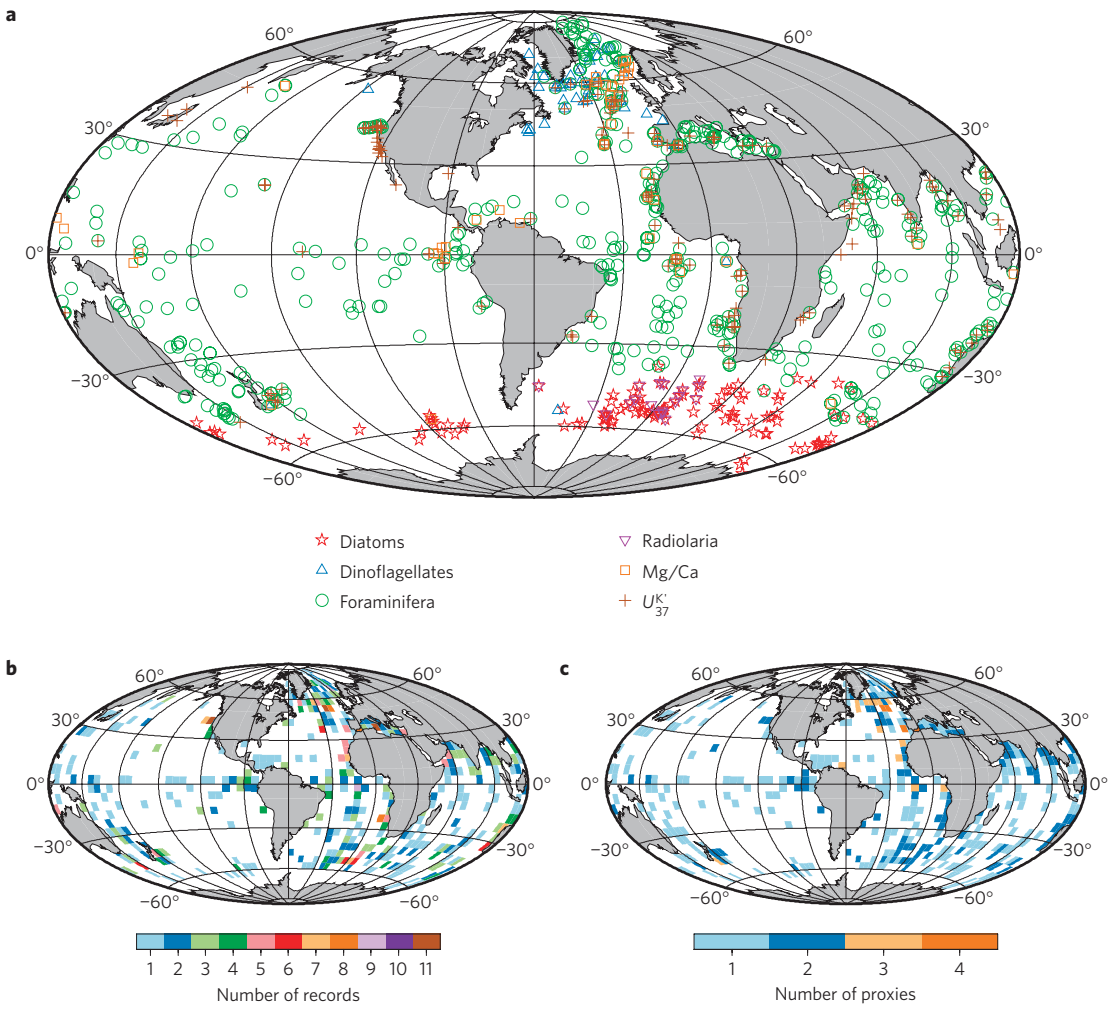

Figure 1 | MARGO data coverage. a, Distribution of data points. **b**, Number of proxy records per 5° × 5° grid cell. **c**, Number of different proxy types per 5° × 5° grid cell.

might indicate that the seasonality of the alkenone production has changed through time[15].

The best convergence between the various proxy estimates occurs within the 30° S–30° N band (Figs 3 and 4). Strong inter-basin differences as well as clear west–east gradients within each basin mark the equatorial oceans, although anomalies are smaller in the Pacific and Indian Ocean than in the Atlantic. Tropical cooling is more extensive than that proposed by CLIMAP. Existing AO-GCM LGM simulations (http://pmip2.lsce.ipsl.fr/) exhibit either no significant west–east gradient in the tropics, or much weaker and even reverse west–east gradients (see Supplementary Information, Tables S1,S2, Figs S3,S4). Discrepancies between these LGM simulations and MARGO data may result from the fact that some forcing factors, such as glacial dust and aerosol distribution, were not included in the LGM simulations[7]. However, even in simulations of present-day conditions, it is difficult for state-of-the-art climate models to resolve the observed west–east gradients in the tropical and subtropical oceans[16] and current climate models produce discordant simulations of present-day and future climate in the tropics[17]. In this context, MARGO's robust LGM results in tropical latitudes could be extremely useful in identifying the causes for the models' divergent results.

Other remarkable features of the tropical reconstructions are a 1–3 °C cooling of the western Pacific warm pool, which is supported by three available proxies[10,18–20], and a 1–3 °C cooling off northwest Australia that suggests an ongoing transport of warm waters along the Indonesian throughflow warm water route[19]. The contracted subtropical gyres in the Atlantic Ocean experienced little cooling in their centre (<−2 °C). In the Pacific, parts of both the northern and southern subtropical gyres may have been warmer than at present by up to 1–2 °C, as suggested by the few available data points. Interestingly, this feature, which was also reconstructed by CLIMAP but has attracted significant controversy, is not simulated by any of the recently available AO-GCM simulations[7].

Large cooling of the eastern boundary current (EBC) systems in the Southern Hemisphere is reconstructed by all proxies, making this a very robust feature of the climate and ocean circulation during the LGM (Fig. 4). This pattern is consistently recorded by foraminiferal assemblages and by the few available Mg/Ca estimates[20]. It is less prominent in the annual average SST reconstructions from alkenones (Figs 2,4). The alkenone-derived LGM values for EBC systems generally seem only moderately colder than the present day (<−2 °C), although new $U^{K'}_{37}$ estimates from the southeastern Pacific not yet considered in the MARGO compilation reveal a 5–6 °C cooling off Chile[21,22]. Such cooling was not strongly present in the CLIMAP reconstruction, but documented by more recent foraminiferal reconstructions[23,24]. The large EBC cooling could have resulted from enhanced Ekman pumping, the upwelling of colder water along the continental margins and, in the case of the eastern South Atlantic, enhanced

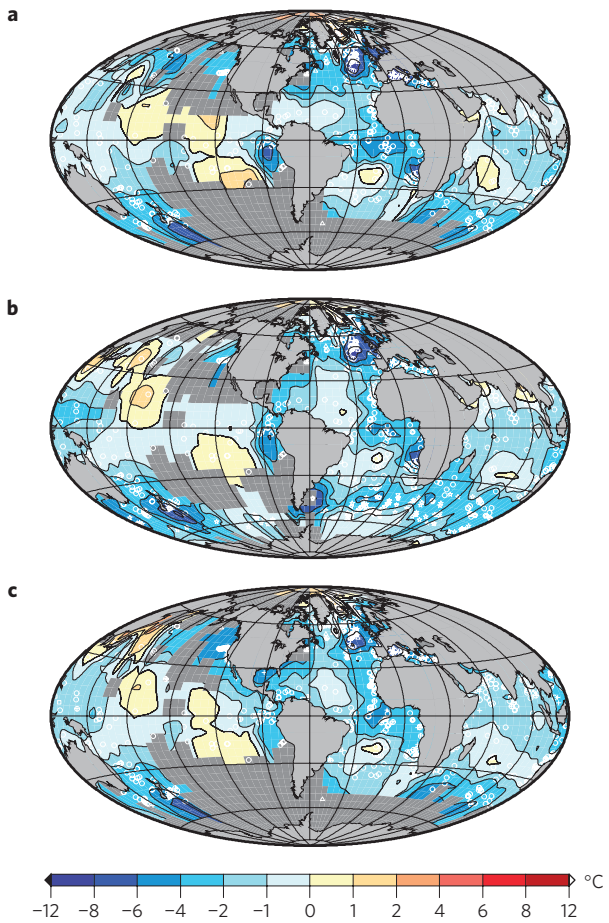

Figure 2 | Maps of reconstructed LGM sea surface temperature anomalies. Anomalies are computed as LGM–WOA98 (ref. 12) values. **a**, Northern Hemisphere summer (July–August–September). **b**, Northern Hemisphere winter (January–February–March). **c**, Annual mean. The symbols show the location and proxy type of the original available data (see Fig. 1). Note the uneven spacing of the diverging colour scheme and isotherms.

advection of subpolar waters into the Benguela current[18,25]. This could in turn result from a general increase in wind strength during glacials and a northward shift in the westerlies and Southern Ocean frontal systems in response to increased sea ice extent around Antarctica[26] (Fig. 2).

In the Southern Ocean, proxy data indicate a northward shift of the polar front during the LGM to a position at 45° S (ref. 26), associated with a −2 to −6 °C cooling during glacial austral summer relative to today. Estimates from siliceous microfossil assemblages are supported by foraminiferal transfer function results, notably in the southern Indian Ocean, where most Southern Ocean foraminifera data points are located[19]. We note that the Southern Ocean and the subtropical South Atlantic and Pacific are regions where large disagreements occur among the latest AO-GCM LGM simulations[7], ranging from no cooling to anomalies exceeding −10 °C (see Supplementary Information, Table S2, Figs S3,S4).

Analysis of the entire multiproxy MARGO data set yields average mean annual anomalies computed from blocks between 90° S–90° N (Table 1) of −2.4±2.2 °C in the Atlantic, −1.6±1.1 °C in the Indian, −1.5 ± 1.8 °C in the Pacific and −1.9 ± 1.8 °C for the global ocean. The average mean annual cooling in the 15° S–15° N tropical band is more pronounced in the Atlantic (−2.9 ± 1.3 °C) and less pronounced in the Indian (−1.4 ± 0.7 °C) and Pacific (−1.2 ± 1.1 °C) oceans, resulting in −1.7 ± 1 °C for the global ocean. The relatively large uncertainties associated with basin-wide averages (see the Methods section) are caused by the high proportion of regions not covered by proxies; they are not the result of method-specific uncertainties nor do they reflect discrepancies between estimates by different proxies. They are due to the fact that the LGM oceans were thermally highly structured with large gradients across small distances. This observation clearly highlights the danger of extrapolating individual LGM SST reconstructions into global fields.

The average mean annual cooling obtained for the tropical Atlantic (Table 1) is −2.9 ± 1.3 °C. This is indistinguishable from the value obtained by ref. 27 for the 20° S–20° N band (3.0 °C) and thus confirms the GLAMAP reconstructions that were based solely on faunal assemblages of foraminifera[24,28]. Using CLIMBER-2 model results as in ref. 27, MARGO SST synthesis translates into a range of climate sensitivities of 1–3.6 °C. However, this result is model dependent. For instance, the MIROC3.2 model shows an asymmetry in climate sensitivity calculated by decreasing rather than increasing the greenhouse gases, which indicates that direct estimates of climate sensitivity from the LGM are likely to underestimate the future climate sensitivity for the coming centuries[29]. More generally, ref. 1 showed that for current state-of-the-art models, there is no linear relationship between LGM cooling and temperature change for a doubling of the pre-industrial atmospheric CO_2 concentration.

With the advent of the multiproxy method, we have not only been able to produce a new reconstruction of the glacial ocean surface, but also to deliver uncertainty estimates (see Supplementary Information, Figs S1,S2). Taken together, this yields new observational bounds on the sensitivity of the Earth's climate system, with the perspective of improving existing climate models that are being used in the assessment of ongoing and future climate change. We note, however, that uncertainties in model forcing and model representations of climate mechanisms and feedbacks complicate the attribution of model–data discrepancies and that the climate sensitivity depends on the climate state and forcing[1]. This situation clearly calls for further advances in the use of palaeo-proxy data to constrain coupled climate models. More specifically, MARGO global multiproxy synthesis demonstrates that LGM climate was characterized by large east–west gradients at tropical latitudes and in the North Atlantic. These essential features reflect major changes in oceanic and atmospheric circulation, but are not captured by existing AO-GCM LGM simulations. Future work will need to identify the exact causes for these model–data discrepancies to improve our understanding of past and present ocean and atmosphere circulation, and our ability to predict future climate change.

Methods

Contour mapping. Calculation of 5° × 5° block averages yields a grid coverage of ~20% for the global ocean (varying between ~14% for the Pacific and ~25% for the Atlantic and Indian oceans), whereby ~30% of the grid cells with data combine SST reconstructions by more than one proxy. For illustrative purposes, the block averages were interpolated using the near-neighbour program of Generic Mapping Tools[30] Version 4. The search radius was set to 2,000 km. The contour maps were prepared using Generic Mapping Tools Version 4.

Error assessment. We assume that the uncertainty inherent to the WOA98 data[12] is much smaller that in the LGM reconstructions so that the uncertainty of the LGM–WOA98 anomalies is practically identical to the uncertainty of the individual LGM estimates.

To assess the error on individual LGM estimates, we use a conservative approach taking into account (1) the error of the calibration for each proxy; (2) the number of samples per core on which the LGM SST reconstruction is based; (3) the quality of the age model for each core; (4) the uncertainty due to the stationarity through time and in space of the calibration error, defined specifically for each proxy.

The error due to the calibration method can be quantified as the standard error of the residuals of the calibration equation, or as the root-mean-squared error of prediction (RMSEP) determined by holding a portion of the calibration

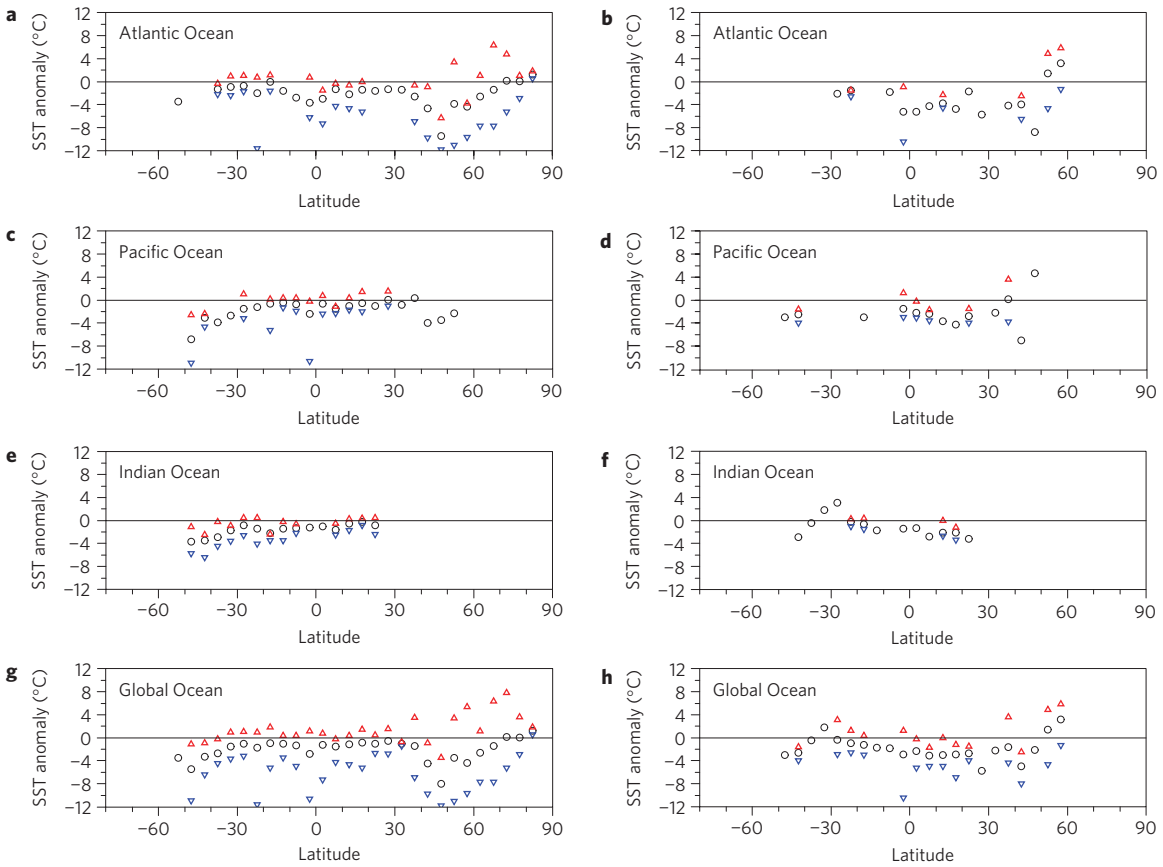

Figure 3 | Latitudinal averages of estimated LGM SST anomalies derived from microfossil and geochemical proxies. SST anomalies derived from foraminifera and dinocyst assemblages (**a**,**c**,**e**,**g**) and from foraminifera Mg/Ca ratio and alkenones $U^{K'}_{37}$ (**b**,**d**,**f**,**h**). Arithmetic averages (circles), minima (red triangles) and maxima (blue triangles) anomalies are shown for 5° latitude bands. Samples from the Southern Ocean, between 70° W and 20° E were assigned to the Atlantic Ocean, between 20 and 150° E to the Indian Ocean and between 150° E and 70° W to the Pacific Ocean. Samples from the Mediterranean were only used to calculate global latitudinal averages.

data set back, developing the predictor based on the remaining part of the data and applying it on the held-back data[18]. For the MARGO compilation, the calibration errors/RMSEPs (1σ) range typically between 1 and 1.5 °C (see Supplementary Information, Table S3–S8).

The representativeness of a LGM SST estimate at a given site depends on the number of samples per core on which the LGM SST reconstruction is based (a larger number increases the representativeness) and on the quality of the age model for each core. These uncertainties are incorporated in the quality flag for number of samples, q_{num}, and in the quality level of the age model, q_{str}, as defined in ref. 5. Similarly, the uncertainty due to the stationarity through time and in space of the calibration error is incorporated in the SST reconstruction reliability flag, q_{rel}, defined specifically for each proxy and reflecting, for example, possible no-analogue situations and known regional or sedimentological bias. These three semi-quantitative flags can be averaged to produce a mean reliability index: $q = (0.75^{*}q_{str} + q_{num} + q_{rel})/2.75$, where q_{str} ranges from 1 to 4 (ref. 5) and q_{num} and q_{rel} range from 1 to 3 (see Supplementary Information). The uncertainty of each LGM SST reconstruction is then calculated as a function of the calibration error, σ_{CAL}, and the reliability index:

$$\sigma_{LGM} = \sigma_{CAL} \cdot q.$$

To estimate the errors of LGM anomalies for individual blocks, $\sigma_{B\text{-}LGM}$, we consider the uncertainty of individual SST reconstructions and the degree of convergence among the SST estimates within each block. Assuming Gaussian error propagation and using quality flags for weighting the block mean, we obtain:

$$\sigma_{B\text{-}LGM} = \frac{\sqrt{\sum_{i=1}^{n}\left(w_i \cdot \sigma_{LGM,i}\right)^2}}{\sum_{i=1}^{n}(w_i)},$$

where w_i is the inverse of the average reliability index.

The uncertainty due to the degree of convergence among the SST estimates within each block can be estimated by their standard deviation, $\sigma_{B\text{-}VAR}$. The resulting estimate of block mean uncertainty, σ_B, is then the combination of the two errors:

$$\sigma_B = \sqrt{\sigma^2_{B\text{-}LGM} + \sigma^2_{B\text{-}VAR}}.$$

The uncertainty of the regional averages, $\sigma_{REG\text{-}B}$, is a function of the uncertainty values for individual blocks, weighted by the area of the blocks, and the number of blocks:

$$\sigma_{REG\text{-}B} = \frac{\sqrt{\sum_{i=1}^{n}\left(a_i \cdot \sigma_{B,i}\right)^2}}{\sum_{i=1}^{n}(a_i)},$$

where a_i is the area of each block i.

However, only a fraction of the total number of blocks per zone have a SST value assigned to them. The uncertainty of the mean thus has to be increased by the uncertainty due to the unknown SST values. This uncertainty is a function of the variance among the SST values for the blocks: in regions with relatively homogeneous SST anomaly distribution, it is less likely that the unknown blocks will have a large effect on the regional mean than in areas with large variations in SST anomalies. Therefore, the uncertainty due to the unknown blocks can be approximated by the standard deviation among the block means within each zone, $\sigma_{REG\text{-}VAR}$, and this uncertainty can be combined with $\sigma_{REG\text{-}B}$ in the following way:

$$\sigma_{REG} = \sqrt{\sigma^2_{REG\text{-}B} + \left(\frac{N-n}{N}\right)\sigma^2_{REG\text{-}VAR}},$$

where N is the total number of blocks and n is the number of blocks with data.

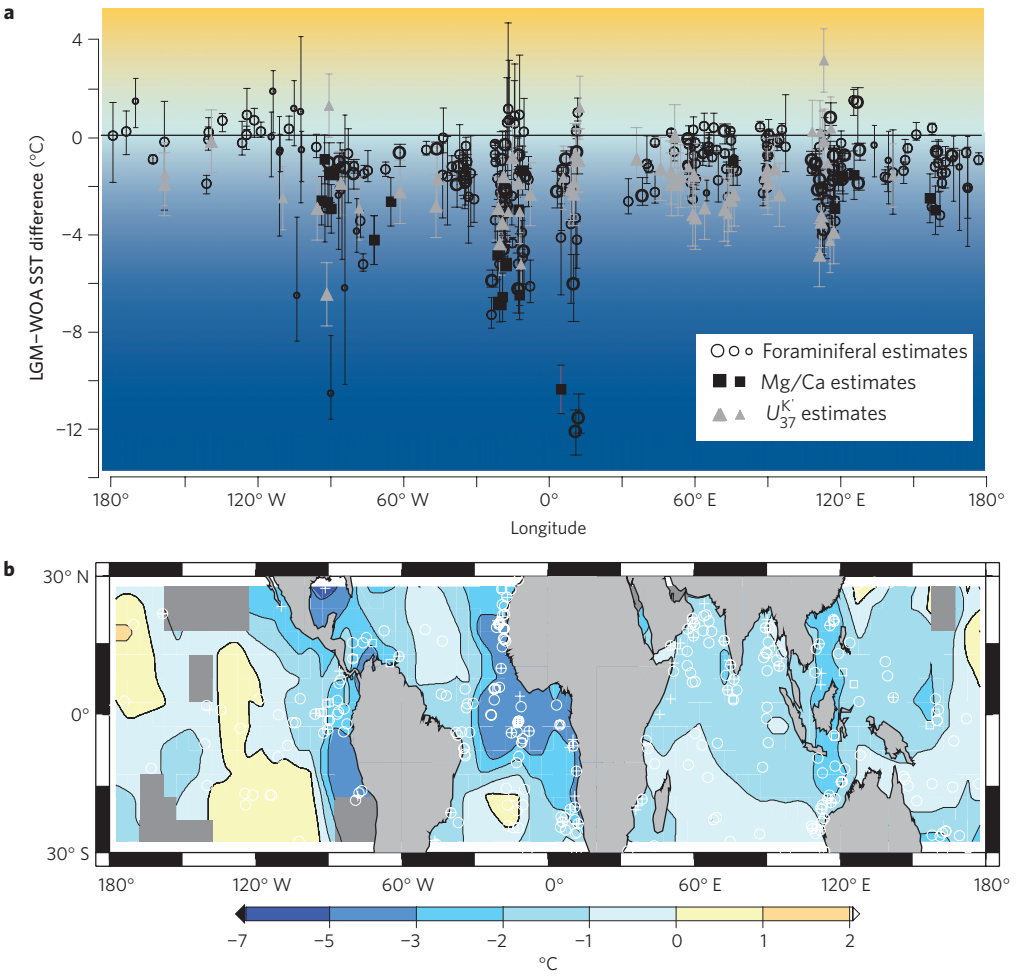

Figure 4 | Map and longitudinal averages of LGM SST annual mean anomalies for the 30° S–30° N tropical band. a, Longitudinal averages of the LGM SST annual mean anomalies derived from foraminifera assemblages, foraminifera Mg/Ca and alkenones $U^{K'}_{37}$. The symbol size is proportional to the average of the three quality indices (see Supplementary Information). Error bars indicate RMSEP (Mg/Ca and alkenones-$U^{K'}_{37}$) or range of the estimates by the different statistical techniques (foraminifera assemblages). **b**, Map of gridded (5° × 5°) SST annual mean anomalies showing the location of the data as in Fig. 1.

Table 1 | Regional mean SST anomalies (modern – LGM) based on block-averaged data with reliability weighting.

		Global Ocean		Atlantic Ocean		Indian Ocean		Pacific Ocean	
	Latitude zone	Regional mean (°C)	Total error (°C)	Regional mean (°C)	Total error (°C)	Regional mean (°C)	Total error (°C)	Regional mean (°C)	Total error (°C)
Annual mean	15° S–15° N	−1.7	1	−2.9	1.3	−1.4	0.7	−1.2	1.1
	30° S–30° N	−1.5	1.2	−2.3	1.5	−1.3	0.7	−1.1	1.2
	60° S–60° N	−1.9	1.7	−2.6	2	−1.6	1	−1.5	1.8
	90° S–90° N	−1.9	1.8	−2.4	2.2	−1.6	1.1	−1.5	1.8
JAS*	15° S–15° N	−1.5	1.6	−3	1.9	−1.2	1	−0.9	1.8
	30° S–30° N	−1.3	1.7	−2.3	2.3	−1	1	−0.9	1.7
	60° S–60° N	−1.9	2.1	−2.7	2.7	−1.5	1.3	−1.4	2
	90° S–90° N	−1.8	2.2	−2.5	2.9	−1.5	1.3	−1.4	2
JFM†	15° S–15° N	−1.6	1.4	−2.5	1.7	−1.3	0.8	−1.2	1.7
	30° S–30° N	−1.4	1.6	−2.2	2.1	−1	1	−1.1	1.7
	60° S–60° N	−2	2	−2.8	2.3	−1.8	1.3	−1.6	2.1
	90° S–90° N	−2	2	−2.7	2.4	−1.7	1.3	−1.5	2.1

*JAS: July–August–September.
†JFM: January–February–March.

Received 10 September 2008; accepted 9 December 2008; published online 18 January 2009

References

1. Crucifix, M. Does the Last Glacial Maximum constrain climate sensitivity? *Geophys. Res. Lett.* **33**, doi:10.1029/2006GL027137 (2006).
2. CLIMAP Project Members. The surface of the ice-age Earth. *Science* **191**, 1131–1137 (1976).
3. CLIMAP Project Members. *Seasonal reconstruction of the Earth's surface at the last glacial maximum* (Map Chart Ser. MC-36, Geol. Soc. Am., 1981).
4. Mix, A. C., Bard, E. & Schneider, R. Environmental processes of the ice ages: Land, oceans, glaciers (EPILOG). *Quat. Sci. Rev.* **20**, 627–657 (2001).
5. Kucera, M., Rosell-Melé, A., Schneider, R., Waelbroeck, C. & Weinelt, M. Multiproxy approach for the reconstruction of the glacial ocean surface (MARGO). *Quat. Sci. Rev.* **24**, 813–819 (2005).
6. Kageyama, M. *et al.* Last Glacial Maximum temperatures over the North Atlantic, Europe and western Siberia: A comparison between PMIP models, MARGO sea–surface temperatures and pollen-based reconstructions. *Quat. Sci. Rev.* **25**, 2082–2102 (2006).
7. Braconnot, P. *et al.* Results of PMIP2 coupled simulations of the Mid-Holocene and Last Glacial Maximum—Part 1: Experiments and large-scale features. *Clim. Past* **3**, 261–277 (2007).
8. Bard, E., Rostek, F. & Sonzogni, C. Interhemispheric synchrony of the last deglaciation inferred from alkenone paleothermometry. *Nature* **385**, 707–710 (1997).
9. Trend-Staid, M. & Prell, W. L. Sea surface temperature at the Last Glacial Maximum: A reconstruction using the modern analog technique. *Paleoceanography* **17**, doi:10.1029/2000PA000506 (2002).
10. Rosell-Melé, A. *et al.* Sea surface temperature anomalies in the oceans at the LGM estimated from the alkenone-U^{K}_{37} index: Comparison with GCMs. *Geophys. Res. Lett.* **31**, L03208 (2004).
11. Pflaumann, U. *et al.* Glacial North Atlantic: Sea-surface conditions reconstructed by GLAMAP 2000. *Paleoceanography* **18**, doi:10.1029/2002PA000774 (2003).
12. World Ocean Atlas 1998: <http://ingrid.ldeo.columbia.edu/SOURCES/.NOAA/.NODC/.WOA98/> (NODC, Silver Springs, 1998).
13. de Vernal, A. *et al.* Comparing proxies for the reconstruction of LGM sea-surface conditions in the northern North Atlantic. *Quat. Sci. Rev.* **25**, 2820–2834 (2006).
14. Meland, M. Y., Jansen, E. & Elderfield, H. Constraints on SST estimates for the northern North Atlantic/Nordic Seas during the LGM. *Quat. Sci. Rev.* **24**, 835–852 (2005).
15. Minoshima, K., Kawahata, H. & Ikehara, K. Changes in biological production in the mixed water region (MWR) of the northwestern North Pacific during the last 27 kyr. *Palaeogeogr. Palaeoclimatol. Palaeoecol.* **254**, 430–447 (2007).
16. Large, W. G. & Danabasoglu, Attribution and impacts of upper ocean biases in CCSM3. *J. Clim.* **19**, 2325–2346 (2006).
17. Solomon, S. *et al.* in *Climate Change 2007, Contribution of Working Group I to the Fourth Assessment Report of the Intergovernmental Panel on Climate Change* (eds Solomon, S. *et al.*) 19–91 (Cambridge Univ. Press, 2007).
18. Kucera, M. *et al.* Reconstruction of the glacial Atlantic and Pacific sea-surface temperatures from assemblages of planktonic foraminifera: Multi-technique approach based on geographically constrained calibration datasets. *Quat. Sci. Rev.* **24**, 951–998 (2005).
19. Barrows, T. T. & Juggins, S. Sea-surface temperatures around the Australian margin and Indian Ocean during the Last Glacial Maximum. *Quat. Sci. Rev.* **24**, 1017–1047 (2005).
20. Barker, S., Cacho, I., Benway, H. & Tachikawa, K. Planktonic foraminiferal Mg/Ca as a proxy for past oceanic temperatures: A methodological overview and data compilation for the Last Glacial Maximum. *Quat. Sci. Rev.* **24**, 821–834 (2005).
21. Lamy, F. *et al.* Antarctic timing of surface water changes off Chile and Patagonian ice sheet response. *Science* **304**, 1959–1962 (2004).
22. Kaiser, J., Lamy, F. & Hebbeln, D. A 70-kyr sea surface temperature record off southern Chile (Ocean Drilling Program Site 1233). *Paleoceanography* **20**, doi:10.1029/2005PA001146 (2005).
23. Feldberg, M. J. & Mix, A. C. Sea-surface temperature estimates in the Southeast Pacific based on planktonic foraminiferal species; modern calibration and Last Glacial Maximum. *Mar. Micropaleontol.* **849**, 1–29 (2002).
24. Sarnthein, M. *et al.* Overview of Glacial Atlantic Ocean Mapping (GLAMAP 2000). *Paleoceanography* **18**, doi:10.1029/2002PA000769 (2003).
25. Paul, A. & Schäfer-Neth, C. in *The South Atlantic in the Late Quaternary: Reconstruction of Material Budgets and Current Systems* (eds Wefer, G., Mulitza, S. & Ratmeyer, V.) 549–583 (Springer, 2004).
26. Gersonde, R., Crosta, X., Abelmann, A. & Armand, L. K. Sea surface temperature and sea ice distribution of the last glacial Southern Ocean—A circum-Antarctic view based on siliceous microfossil records. *Quat. Sci. Rev.* **24**, 869–896 (2005).
27. Schneider von Deimling, T., Held, H., Ganopolski, A. & Rahmstorf, S. Climate sensitivity estimated from ensemble simulations of glacial climate. *Clim. Dyn.* **27**, 149–163 (2006).
28. Schäfer-Neth, C. & Paul, A. in *The South Atlantic in the Late Quaternary: Material Budget and Current Systems* (eds Wefer, G., Mulitza, S. & Ratmeyer, V.) 531–548 (Springer, 2004).
29. Hargreaves, J. C., Abe-Ouchi, A. & Annan, J. D. Linking glacial and future climates through an ensemble of GCM simulations. *Clim. Past* **3**, 77–87 (2007).
30. Wessel, P. & Smith, W. H. F. New improved version of Generic Mapping Tools released. *EOS, Trans. Am. Geophys. Union* **79**, 579 (1998).

Acknowledgements

We are grateful to M. Kageyama, C. Dumas and J. Y. Peterschmitt for assistance with PMIP2 output files. We thank the HANSE Advanced Study Institute for hosting the first international MARGO workshop in Delmenhorst, Germany, in September 2002 and Fundació Abertis for hosting the second MARGO workshop in Castellet i la Gornal, Spain, in September 2003. We warmly thank the IGBP-PAGES project for its support. The MARGO project is an outcome of the EPILOG working group of IMAGES. C.W. is financially supported by CNRS and INSU.

Additional information

Supplementary Information accompanies this paper on www.nature.com/naturegeoscience. Reprints and permissions information is available online at http://npg.nature.com/reprintsandpermissions. Correspondence and requests for materials should be addressed to C.W.

MARGO Project Members: C. Waelbroeck[1]*, A. Paul[2], M. Kucera[3], A. Rosell-Melé[4], M. Weinelt[5], R. Schneider[5], A. C. Mix[6], A. Abelmann[7], L. Armand[8], E. Bard[9], S. Barker[10], T. T. Barrows[11], H. Benway[6], I. Cacho[12], M.-T. Chen[13], E. Cortijo[1], X. Crosta[14], A. de Vernal[15], T. Dokken[16], J. Duprat[14], H. Elderfield[17], F. Eynaud[14], R. Gersonde[7], A. Hayes[18], M. Henry[15], C. Hillaire-Marcel[15], C.-C. Huang[13], E. Jansen[16], S. Juggins[19], N. Kallel[20], T. Kiefer[17], M. Kienast[21], L. Labeyrie[1], H. Leclaire[1], L. Londeix[14], S. Mangin[14], J. Matthiessen[7], F. Marret[22], M. Meland[16], A. E. Morey[6], S. Mulitza[2], U. Pflaumann[5], N. G. Pisias[6], T. Radi[14], A. Rochon[23], E. J. Rohling[24], L. Sbaffi[25], C. Schäfer-Neth[7], S. Solignac[15], H. Spero[26], K. Tachikawa[9] and J.-L. Turon[14]

[1]LSCE/IPSL, Laboratoire CNRS-CEA-UVSQ, Domaine du CNRS, 91198 Gif-sur-Yvette, France, [2]MARUM—Center for Marine Environmental Sciences and Department of Geosciences, University Bremen, 28334 Bremen, Germany, [3]Institute for Geosciences, University of Tübingen, 72076 Tübingen, Germany, [4]ICREA and Institute of Environmental Science and Technology, Universitat Autònoma de Barcelona, 08193 Bellaterra, Spain, [5]Institute for Geosciences, University of Kiel, 24098 Kiel, Germany, [6]College of Oceanic and Atmospheric Sciences, Oregon State University, Corvallis, Oregon 97331, USA, [7]Alfred Wegener Institute for Polar and Marine Research, 27515 Bremerhaven, Germany, [8]Antarctic Climate and Ecosystem Cooperative Research Centre and CSIRO Marine and Atmospheric Research, Hobart Tasmania 7001, Australia, [9]CEREGE (UMR 6635), Aix-Marseille Université, CNRS, IRD, Collège de France, Europole de l'Arbois, BP80, 13545 Aix-en-Provence, France, [10]School of Earth and Ocean Sciences, Cardiff University, Cardiff CF10 3YE, UK, [11]Research School of Physical Sciences and Engineering, Australian National University, Canberra ACT0200, Australia, [12]CRG Marine Geosciences, University of Barcelona, 08028 Barcelona, Spain, [13]Institute of Applied Geosciences, National Taiwan Ocean University, Keelung 20224, Taiwan, [14]DGO, UMR-CNRS 5805 EPOC, University of Bordeaux I, Talence, France, [15]GEOTOP, University of Québec, PO Box 8888, Montreal H3C 3P8, Canada, [16]Bjreknes Centre for Climate Research, University of Bergen, 5007 Bergen, Norway, [17]Department of Earth Sciences, University of Cambridge, Cambridge CB2 3EQ, UK, [18]Department of Geography, University of Limerick, Ireland, [19]School of Geography, Politics and Sociology, University of Newcastle, Newcastle NE1 7RU, UK, [20]Laboratoire E08/C10, University of Sfax, 3038 Sfax, Tunisia, [21]Department of Oceanography, Dalhousie University, Halifax NS B3H 4J1, Canada, [22]Department of Geography, University of Liverpool, Liverpool L69 7ZT, UK, [23]ISMER, University of Québec, Rimouski G5L 3A1, Canada, [24]National Oceanography Centre, Southampton SO14 3ZH, UK, [25]Geoscience Australia, GPO Box 378, Canberra ACT 2601, Australia, [26]Department of Geology, University of California, Davis, California 95616, USA. *e-mail: claire.waelbroeck@lsce.ipsl.fr.